2019 2nd IEEE International Conference on Soft Robotics (RoboSoft)
COEX, Seoul, Korea, April 14-18, 2019

# Dynamically Closed-Loop Controlled Soft Robotic Arm using a Reduced Order Finite Element Model with State Observer

Robert K. Katzschmann*, Maxime Thieffry*, Olivier Goury, Alexandre Kruszewski,
Thierry-Marie Guerra, Christian Duriez, Daniela Rus

***Abstract*— This paper presents a computationally efficient method to model and simulate soft robots. Finite element methods enable us to simulate and control soft robots, but require us to work with a large dimensional system. This limits their use in real-time simulation and makes those methods less suitable for control design tools. Using model order reduction, it is possible to create a reduced order system for building controllers and observers. Model reduction errors are taken into account in the design of the low-order feedback, and it is then applied to the large dimensional, unreduced model. The control architecture is based on a linearized model of the robot and enables the control of the robot around this equilibrium point. To show the performance of this control method, pose-to-pose and trajectory tracking experiments are conducted on a pneumatically actuated soft arm. The soft arm has 12 independent interior cavities that can be pressurized and cause the arm to move in three dimensions. The arm is made of a rubber material and is casted through a lost-wax fabrication technique.**

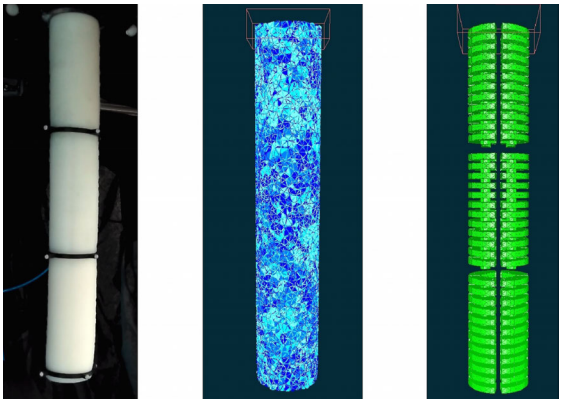

Fig. 1. Robotic arm studied: Real soft arm prototype (left), simulated model of the soft arm shown as a finite element mesh (center), and the pneumatically actuated interior cavities of the arm (right).

## I. Introduction

Soft robots are difficult to model and simulate. We provide a data-driven solution for modeling soft robots and connect the model to an efficient simulation engine using model order reduction. This approach provides an efficient and realistic method to develop controllers for soft robots in simulation. We validate the approach on a physical prototype.

Soft robots take their inspiration from nature. Natural organisms interact with the external world through the elasticity of their bodies while they can perform tasks in a dynamic manner. This is why researchers design soft robots with elastic bodies [1], for example soft robotic fish [2], soft grippers [3], soft worms [4], and soft octopuses [5].

We are motivated by the hope to create soft-bodied robots that can perform similarly well in terms of agility in motion and compliance during interactions. To enable these motions and interactions, we need suitable soft robotic prototypes and appropriate models to control these robots dynamically. Both the creation of fast actuated soft robots as well as tractable dynamic modeling are challenging. Nevertheless, a soft robot has to robustly manage the intelligence embedded in its complex structure in order to generate desirable behaviors.

Control strategies suitable for dynamically moving soft robots have been challenging to develop. One difficulty in particular is to make good use of a mathematical formulation for the soft robotic model. This requires us to find a way of taking into account the infinite dimensions of the robot's state space [6] without exploding in dimensionality and rendering the model unsuitable for control.

To avoid the computation of a complex and hard to exploit model, solutions have been proposed using open-loop data-driven approaches [7], or a combination of learning and model-based control [8]. Yet, only a few modelling techniques for soft robots have been used to design dynamic controllers. Dynamic control methods taking into account contacts between the soft body and its environment have been proposed in [9], [10]. The control method is based on a Piece-wise Constant Curvature model combined with an augmented rigid body model. The experimental results are shown on a two-dimensional [9] and a three-dimensional soft robotic arm [10]. While computationally efficient, the approach is specific to robots with symmetric geometries.

The use of simulation shortens the development time of a robotic system. Simulation enables researchers to quickly test out and iterate on different designs, actuation methods and control approaches. Finite element methods (FEM) are one way to achieve this goal. A simulation software based on SOFA [11] proposes to model soft robots using FEM [12]. The software requires the discretization of the

*The authors contributed equally to this work.

R.K. Katzschmann, and D. Rus are with the Computer Science and Artificial Intelligence Laboratory, Massachusetts Institute of Technology, 32 Vassar St., Cambridge, MA 02139, USA, robert@katzschmann.de, rus@csail.mit.edu

M. Thieffry, O. Goury, A. Kruszewski and C. Duriez are are in Defrost team, Inria, university of Lille, Centrale Lille, CRIStAL - Centre de Recherche en Informatique Signal et Automatique de Lille - UMR 9189, France, maxime.thieffry@inria.fr

M. Thieffry and T.M. Guerra are with the Polytechnic University Hauts de France, CNRS, UMR 8201 - LAMIH F-59313 Valenciennes, France.

robot's geometry into a finite element mesh, based on which the continuum mechanics and soft material theories are then solved. Boundary conditions are defined using constraints for both contacts and the robot's actuators.

The use of numerical methods often leads to large dimensional systems, as the precision of the model is linked to the number of nodes of the mesh. To tackle this problem, model order reduction is used to obtain a system of acceptable dimensions. Reduced order modelling for soft robots has been studied in [13] and [14] and a reduced-order controller based on FEM has been proposed in [15]. So far, the method has only been tested on a soft foam beam actuated with only two tendon cables applying only point forces. Multiple pressure loads or other actuation types had not been considered yet. In this paper we propose to adapt and validate the modeling and control methods to a pneumatically pressurized soft arm, dynamically actuating a total of 12 individually actuated cavities. In summary, this work contributes:

- Adaptation of a dynamic controller and observer based on a reduced-order model of a non-linear FEM model.
- Validation of the FEM-based closed-loop control approach on a three-dimensional soft robotic arm through pose-to-pose and trajectory tracking experiments.

## II. Model

In this section, we first describe the geometric model of the soft robot studied in this paper. This is followed by a description of the FEM-based dynamic model and the model-order reduction approach. This part is done using a unified software framework dedicated to modeling and control of soft robots [12]. This software uses non-linear continuum mechanics to build a model of a soft robot. For our control application, this model is then linearized around an equilibrium. Finally, we describe how this modeling method is applied to the soft robot.

### A. Geometry

The soft robot used in this study is a concatenation of cylindrical soft actuator segments. Each segment has inflatable cavities shaped as a series of thin ribs. This three dimensional design is an extension of a previously presented planar design in form of a soft fish tail [2], [16] and in form of soft finger [17], [18]. The planar design was characterized and compared to other cavity shapes in a design study [19]. The arm shown in here is also a 3D extension of a soft planar robotic arm used for autonomous object manipulation [20] and dynamic planar motions [9]. The design of this arm improves over previous three-dimensional designs [21] through its circular arranged set of actuated ribs.

Specifically, the arm is composed of three segments with four inflatable cavities in each segment. Each cavity has a ribbed interior geometry that allows for more bending and less radial inflation when compared to a purely cylindrical cavity design. Each ribbed cavity consists of 16 ribs connected by a thin connecting channel between those 16 ribs. Each rib is $3.1\,\mathrm{mm}$ high and between each rib is a gap of $3\,\mathrm{mm}$. The thickness between each rib and the outer surface of a segment is only 2mm.

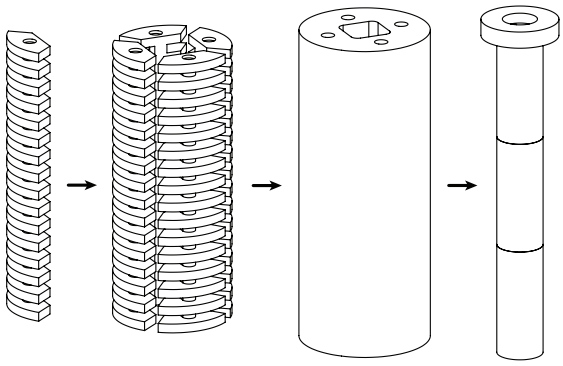

Fig. 2. Geometric model of the soft arm. From left to right: the shape of a single ribbed cavity; circular arrangement of four cavities; soft arm segment with embedded cavities; concatenation of three actuated segments plus passive base.

The independent pneumatic actuation of the arm's segments is achieved through an array of 12 proportional valves. A motion tracking system provides real-time measurements of four marked points placed around the perimeter of the arm at the intersecting planes between each segment.

### B. FEM Model with Dynamics

For the complex geometry of a deformable robot, it is challenging to adequately describe and model its continuously deforming structure without using a large state space. We discretize the structure into a mesh of finite elements and derive our model describing the structural compliance, damping, and dynamics based on Newton's second law:

$$\mathcal{M}(q)\dot{v} = \mathcal{P}(q) - \mathcal{F}(q,v) + \mathcal{H}^T(q)z(t) \qquad (1)$$

where $q \in \mathbb{R}^n$ represents all degrees of freedom of the model. Since our solution is based on the finite element method, the degrees of freedom of the system are the nodes of the mesh and each node can move in the three directions of Cartesian space. The dimension $n$ of $q$ is equal to $3 \times \mathcal{N}$, where $\mathcal{N}$ is the number of nodes of the mesh. $\mathcal{M}(q) : \mathbb{R}^n \to \mathbb{R}^{n\times n}$ is the mass matrix, $v = \dot{q}$ is the velocity vector, $\mathcal{F}(q,v)$ represents the internal forces and $\mathcal{P}(q)$ gathers all the known external forces. As we consider as external forces only the gravitational field, $\mathcal{P}(q)$ is constant and $\mathcal{P}(q) = \mathcal{P}$. $\mathcal{H}^T(q)z$ is the actuators contribution: $\mathcal{H}^T(q)$ contains the direction of the actuators' forces and $z$ is their amplitude.

To model the deformations of soft robots, we are using deformable models able to deal with elastic behavior for large displacements: the robot goes back to its initial shape when the actuation vanishes and the parameters of the materials are given by the Young's modulus and the Poisson's ratio of Hooke's law. This law makes the assumption of linearity in material response due to a load. To model the deformation of soft robots, the FEM integrates over the mesh of the robot the constitutive law of its material. Lagrange multipliers are used to define boundary conditions to model the actuation contribution or the contacts with the environment.

Let $q_0 \in \mathbb{R}^n$ be a stable equilibrium that could be obtained using an inverse problem. This configuration $q_0$ is induced by $\mathcal{P}$ and $z(t) = z_0$, that is $q_0$ is solution to

$$0 = \mathcal{P} - \mathcal{F}(q_0, 0) + \mathcal{H}^T(q_0) z_0 \tag{2}$$

Adding Equation (2) to the right-hand side of Equation (1):

$$\begin{aligned} &\mathcal{M}(q)\dot{v} = \mathcal{P} - \mathcal{F}(q,v) + \mathcal{H}^T(q)z(t) - \mathcal{P} + \mathcal{F}(q_0,0) - \mathcal{H}^T(q_0)z_0 \\ &\quad \Leftrightarrow \\ &\mathcal{M}(q)\dot{v} = \mathcal{F}(q_0,0) - \mathcal{F}(q,v) + \mathcal{H}^T(q)z(t) - \mathcal{H}^T(q_0)z_0 \end{aligned} \tag{3}$$

We can approximate the internal forces $\mathcal{F}$ with a first order Taylor expansion around this equilibrium point:

$$\mathcal{F}(q,v) \approx \mathcal{F}(q_0,0) + \left.\frac{\partial \mathcal{F}(q,0)}{\partial q}\right|_{q=q_0} (q - q_0) + \left.\frac{\partial \mathcal{F}(q_0,v)}{\partial v}\right|_{v=0} v \tag{4}$$

where $\frac{\partial \mathcal{F}(q,v)}{\partial q} = \mathcal{K}(q,v)$ is the compliance matrix, and $\frac{\partial \mathcal{F}(q,v)}{\partial v} = \mathcal{D}(q,v)$ is the damping matrix. Using Rayleigh's definition of damping, the matrix $\mathcal{D}(q,v)$ can be defined as:

$$\mathcal{D}(q,v) = \alpha M(q) + \beta K(q,v) \tag{5}$$

where $\alpha$ and $\beta$ are respectively the mass and stiffness coefficient of damping. By definition, mass, compliance and damping matrices are positive definite. With these notations, equation (3) becomes:

$$\mathcal{M}(q)\dot{v} \approx -\mathcal{K}(q_0,0)(q-q_0) - \mathcal{D}(q_0,0)v + \mathcal{H}^T(q)z(t) - \mathcal{H}^T(q_0)z_0 \tag{6}$$

Let $d$ be the displacement vector defined by:

$$d = q - q_0 \tag{7}$$

The equation of motion around an equilibrium point $q_0$ is thus given by the following relation:

$$\mathcal{M}(q)\dot{v} \approx -\mathcal{K}(q_0,0)d - \mathcal{D}(q_0,0)v + \mathcal{H}^T(q)z(t) - \mathcal{H}^T(q_0)z_0 \tag{8}$$

Around an equilibrium point $q_0$, let us consider $\mathcal{M} = \mathcal{M}(q_0,0)$, $\mathcal{D} = \mathcal{D}(q_0,0)$, $\mathcal{K} = \mathcal{K}(q_0,0)$ and $\mathcal{H}(q_0) = \mathcal{H}(q) = \mathcal{H}$. Defining the new input vector $u(t)$ as $u(t) = z(t) - z_0$, system (8) can be linearized to:

$$\begin{cases} \dot{x} = \underbrace{\begin{pmatrix} -\mathcal{M}^{-1}\mathcal{D} & -\mathcal{M}^{-1}\mathcal{K} \\ I & 0 \end{pmatrix}}_{A} x + \underbrace{\begin{pmatrix} \mathcal{M}^{-1}\mathcal{H}^T \\ 0 \end{pmatrix}}_{B} u \\ y = Cx \end{cases} \tag{9}$$

where $x = \left(v^T \, d^T\right)^T$, $x \in \mathbb{R}^{2n}$ and system matrices are large-scale sparse matrices, i.e. $A \in \mathbb{R}^{2n\times 2n}, B \in \mathbb{R}^{2n\times m}, C \in \mathbb{R}^{p\times 2n}$, where $m$ is the number of actuators and $p$ the number of outputs.

### C. Model Order Reduction

The accuracy of the FEM is highly influenced by the number of mesh nodes, leading to models with a very large number of degrees of freedom. The high number of dimensions renders this approach unsuitable for the synthesis of model-based control laws. Systems with thousands of decision variables can not be tackled with current control design tools. That is why model reduction is used to obtain a system of reduced dimension. This simplified system can then be used to design both a controller and an observer. Projection-based model order reduction consists of finding two projectors $V \in \mathbb{R}^{2n\times 2n}$ and $W \in \mathbb{R}^{2n\times 2n}$ to decompose the large-scale vector $x$ into a reduced order state $x_r \in \mathbb{R}^r$ and a neglected state $x_{\bar{r}} \in \mathbb{R}^{2n-r}$.

$V = (V_r \; V_{\bar{r}}) \in \mathbb{R}^{2n\times 2n}$ and $W = (W_r \; W_{\bar{r}}) \in \mathbb{R}^{2n\times 2n}$ are used to compute a reduced order state $x_r \in \mathbb{R}^r$ and a neglected state $x_{\bar{r}} \in \mathbb{R}^{2n-r}$. Their relationships are defined as:

$$x = \begin{pmatrix} V_r & V_{\bar{r}} \end{pmatrix} \begin{pmatrix} x_r \\ x_{\bar{r}} \end{pmatrix} \tag{10}$$

and

$$\begin{aligned} x_r &= W_r^T x \\ x_{\bar{r}} &= W_{\bar{r}}^T x \end{aligned} \tag{11}$$

.

Projectors are orthogonal to each other, it holds $W_r^T V_r = I$ and $W_r^T V_{\bar{r}} = 0$. Thus, the system's dynamics defined in (9) combined with the projectors defined in (10) and (11) can be described as:

$$\begin{cases} \dot{x}_r = W_r^T A V_r x_r + W_r^T B u + W_r^T A V_{\bar{r}} x_{\bar{r}} \\ \dot{x}_{\bar{r}} = W_{\bar{r}}^T A V_{\bar{r}} x_{\bar{r}} + W_{\bar{r}}^T B u + W_{\bar{r}}^T A V_r x_r \\ y = C V_r x_r + C V_{\bar{r}} x_{\bar{r}} \end{cases} \tag{12}$$

Different results exist in the literature for linear model reduction, like balanced truncation or iterative tangential interpolation, but the only method suitable for non-linear systems is the Proper Orthogonal Decomposition(POD) [22].

Since soft robots can largely deform, we are required to choose an approach to model order reduction that can in the future also account for non-linear behaviors. Therefore, POD is used to perform the model reduction. The POD proposes to represent the high-dimensional model of the structure within a subspace of much smaller dimension. An offline simulation is performed where all the potential movements of the structure studied are sampled and stored in snapshots. This step is computationally intensive, since fine simulations are performed, but it is performed only once to build the reduced order model. Singular value decomposition (SVD) and a truncation - depending on the decay rate of the singular values - condense the snapshot space in a reduced basis.

For applications with dynamic motions, we use simulations to save snapshots of the robot's acceleration for different configurations. Note that different choices of snapshots can be made to perform the reduction; i.e. velocity or position could be used instead of acceleration. From our initial testing, we found that using acceleration was giving us more accurate results. Different combinations of actuation - that we consider exhaustively in the desired range of actuation - are applied to the robot. The reduced order model will only be accurate for the positions that we took into account during a snapshot experiment. At each time step, the matrix

$S$ is enriched with the value of the acceleration vector of the robot. We therefore obtain a snapshot matrix $S$:

$$S = \begin{pmatrix} \dot{v}_{t0} & \dot{v}_{t1} & \dots & \dot{v}_{tf} \end{pmatrix} \tag{13}$$

Matrices $V$ and $W$ are then obtained performing a singular value decomposition (SVD) of $S$:

$$S = \mathcal{U}\Sigma\mathcal{V} \tag{14}$$

Depending on the decay rate of the singular values of $\Sigma$, a low-order approximation can be computed by

$$\begin{aligned} T_r &= \begin{pmatrix} \mathcal{U}_1 & \dots & \mathcal{U}_r \end{pmatrix} \\ T_{\bar{r}} &= \begin{pmatrix} \mathcal{U}_{r+1} & \dots & \mathcal{U}_n \end{pmatrix} \end{aligned} \tag{15}$$

Finally, the projectors $V$ and $W$ are defined as:

$$\begin{aligned} V_r = W_r &= \begin{pmatrix} T_r & 0 \\ 0 & T_r \end{pmatrix} \\ V_{\bar{r}} = W_{\bar{r}} &= \begin{pmatrix} T_{\bar{r}} & 0 \\ 0 & T_{\bar{r}} \end{pmatrix} \end{aligned} \tag{16}$$

For a complete view of this model reduction algorithm, see Algorithm 1 in [14]. This methodology provides us with a low dimensional state $x_r$ and a reduced order system which is compatible with the design of an output feedback control law. In both cases, the aim is to use only $x_r$ to control the whole state dynamics described in (9) while studying the impact of the neglected state $x_{\bar{r}}$ on the system.

### D. Model Application to the Soft Arm

The modeling and simulation part of this work is done using the SOFA framework - an open source framework targeted at the simulation of deformable materials - with the SoftRobotPlugin [12] and Model Order Reduction[1] plugins. These tools enable real-time simulation and control of soft robots using the FEM described in the previous subsections.

The mesh of the soft arm described in Section IV-A is presented in Figures 1 and 3. The mesh consists of $45116$ tetrahedra and $11810$ nodes. The state vector of the dynamic model has a length of $11810 \times 6 = 70860$. The model implemented in SOFA is non-linear, but in order to design the dynamic controller, the model of the arm is linearized around its resting position. Using the model reduction algorithm presented above, the large-scale dynamic model (9) is transformed to a lower order model (12) with $x_r \in \mathbb{R}^{10}$, that means we consider the five first singular values of the snapshots. These singular values decrease rapidly and the first five represent $71.4\%$ of the singular values of $\Sigma$.

[1]https://project.inria.fr/modelorderreduction/, see [14]

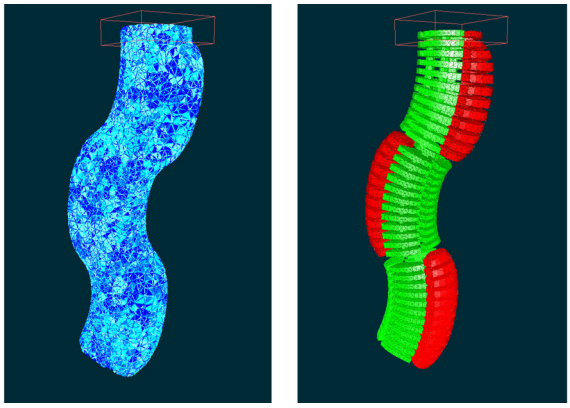

Fig. 3. Exemplary deformation state of the soft arm in simulation.

**Remark 1.** *The simulation of the full order non-linear model, given in equation* (1)*, runs at 1.5 frames per second (fps) on an Intel Core i7 CPU. The low-order system simulates at 25 fps. To run the control algorithm introduced later in equation* (19)*, the simulation platform SOFA is not needed anymore and the frequency of the feedback control loop is constraint by the hardware setup.*

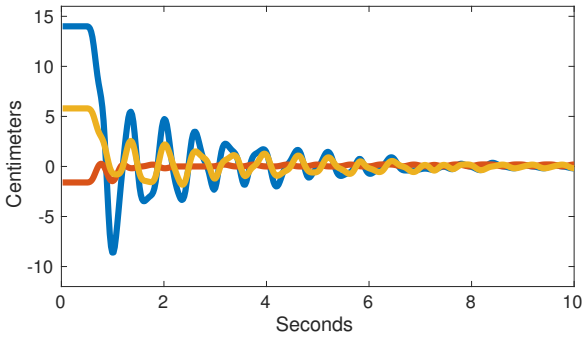


Fig. 4. Open-loop arm experiment starting from an actuated and deformed state going towards a straight, down-hanging arm pose. The graph shows the x (red), y (blue) and z (yellow) positions of the arm's end-effector as it is swinging back and fourth while asymptotically nearing a straight arm pose.

We validate the proposed model by comparing the open-loop behaviour of the simulation to the physical prototype. In the first experiment we release the arm from a deformed shape and let it converge to its resting pose, hanging straight down. The results of this first experiment are shown in Figure 4. Then, a second experiment is done were the robot starts from its rest shape and converges to a deformed position; results are shown in Figure 5. Figure 6 shows the output that presents the maximum absolute error between the simulated model and the real soft arm during the open-loop experiment where the robot goes from an actuated state back to its rest shape. A maximum error of about $3\,\mathrm{cm}$ exists between the simulated results and the real measurements. This corresponds to a relative error of $9.1\%$ in regards to the robot's characteristic length.

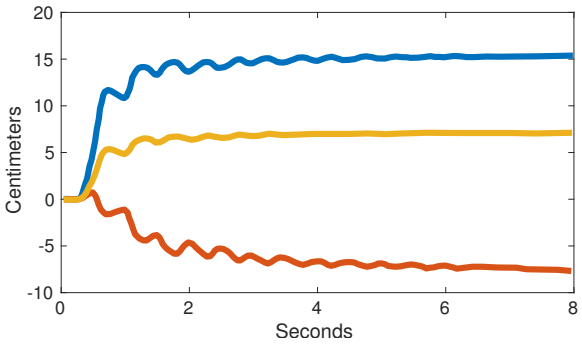


Fig. 5. Open-loop arm experiment, starting from a straight, down-hanging arm pose going towards a deformed state through an open-loop step actuation. The graph shows the x (red), y (blue) and z (yellow) positions of the arm's end-effector as it is swinging back and fourth while asymptotically nearing a straight arm pose.

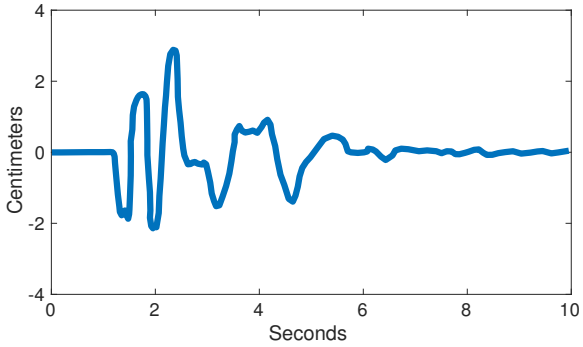


Fig. 6. Maximum error between measurement outputs of simulation and physical experiment for the open-loop experiment where the robot returns from an actuated state back to its straight rest shape.

## III. Observer Based Output Feedback

In the previous section, we presented an FEM model to describe the deformation and dynamics for a soft robot and we described a model order reduction algorithm to address the high dimension of the FEM model. In this section, we describe our approach to an observer-based closed-loop control design that also makes use of the FEM model and the model order reduction.

### A. Observer-based Dynamic Controller

We previously presented a control method for soft robots based on a reduced model and that took into account the reduction error [15]. The idea behind the control design in the work here is to control the dynamics of the reduced system using a feedback control law and ensure the large-scale closed loop stability using Lyapunov theory. To use this control design in practice, where neither $x$ nor $x_r$ are available from sensors, an unknown input observer reconstructs $x_r$ and considers the reduction error as a disturbance. Only $y$ is directly available from the sensors.

The vector $\omega$ gathers the reduction error and is the unknown input to the observer:

$$\begin{aligned} \dot{\hat{x}}_r &= A_r\hat{x}_r + B_r u + F(y - \hat{y}_r) + Z\omega \\ \hat{y}_r &= C_r\hat{x} \end{aligned} \tag{17}$$

where $F$ is the reduced-order observer gain. Let $L \in \mathbb{R}^{m\times r}$ be the feedback matrix of the control law with $m$ being the number of inputs of the system:

$$u = -L\hat{x}_r \tag{18}$$

This reduced order control law with its observer model is then applied to the large-scale system:

$$\begin{cases} \dot{x} = Ax - BL\hat{x}_r \\ y = Cx \end{cases} \tag{19}$$

For the soft arm studied in this work, the reduced order state consists of 10 states, the matrix $L$ is also of dimension $12\times 10$. The computation of this matrix is achieved through a Linear Matrix Inequalities (LMI) problem, with 120 variables and with a stability constraint for the large-scale model.

Stability of the closed-loop is studied using the knowledge of an open-loop Lyapunov function $V(x) = x^T Px$ that is based on the energy of the system, see also [15]. Using projection defined in Equations (10) and (11), it holds:

$$V(x) = x^T Px = \begin{pmatrix} x_r \\ x_{\bar{r}} \end{pmatrix}^T \begin{pmatrix} V_r \\ V_{\bar{r}} \end{pmatrix}^T P \begin{pmatrix} V_r \\ V_{\bar{r}} \end{pmatrix} \begin{pmatrix} x_r \\ x_{\bar{r}} \end{pmatrix} \tag{20}$$

The objective of the LMI problem is to optimize the decay-rate of $V(x)$ with feedback $u = -L\hat{x}_r$ (18). As the Lyapunov function uses the large-scale vector to tune the performances via $x_r$, the stability of the whole model ($x_r$ and $x_{\bar{r}}$) is also guaranteed.

### B. Simulation of the Controlled System

The control algorithm is first tested in simulation. Dynamic control around static positions and trajectory tracking experiments are done to show the capabilities of the methodology, that is the model order reduction and robust control.

*1) Pose-to-Pose Control in Simulation:* A first test is performed where the objective is to drive the simulated soft arm from a deformed shape to its rest position. The comparison of the position of the end-effector for this experiment in open and closed-loop is shown in Figure 7.

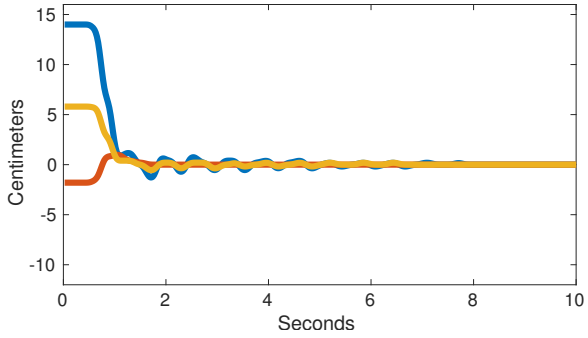


Fig. 7. Simulation of closed-loop control, showing the motion of the end-effector going from an actuated state to the straight resting pose. Red, blue and yellow lines show position of the end-effector along x, y and z axis.

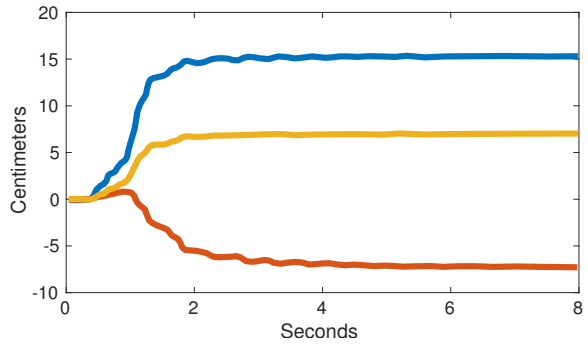


Fig. 8. Simulation of closed-loop control, showing the motion of the end-effector going from the straight resting pose to an actuated state. Red, blue and yellow lines show position along x, y and z axis.

A second set of experiments is conducted where the arm starts from its rest shape position and converges to a deformed position; results are shown in Figure 8.

As one metric for evaluation of the results, we use the integral time absolute error (ITAE) criterion defined as:

$$ITAE = \int_0^T t|e(t)|dt \tag{21}$$

This criterion is used to measure the overshoots and oscillations of the system's response. To compare the controller performances, the value of the ITAE in closed-loop are compared with the one of the open-loop. In addition, the 3% settling time is given for the same experiments in open and closed loop; results are shown in Table I. Results show a maximum gain of 67.53% in ITAE and 58.65% for the settling time. It also shows that the gains are higher when the target position is the position where the model of the robot has been linearized.

TABLE I
CONTROL IN SIMULATION: COMPARISON OF INTEGRAL TIME ABSOLUTE ERROR (ITAE) AND 3% SETTLING TIME IN OPEN AND CLOSED-LOOP IN SIMULATION.

| | to rest position | to curled position |
|---|---|---|
| ITAE in: | | |
| open-loop | 691.52 | 242.19 |
| closed-loop | 224.56 | 209.24 |
| difference in % | 67.53 % | 13.61 % |
| 3% settling-time in: | | |
| open-loop | 6.53 s | 3.52 s |
| closed-loop | 2.7 s | 1.6 s |
| difference in % | 58.65 % | 54.55 % |

*2) Trajectory Tracking in Simulation:* We test our methodology first by conducting trajectory tracking experiments in simulation before later using it on the actual robot. A circular end-effector trajectory is defined for tracking. The results are presented in Figure 9. A maximum absolute error of 1.175 centimeters exists between the reference signal and the simulated output.

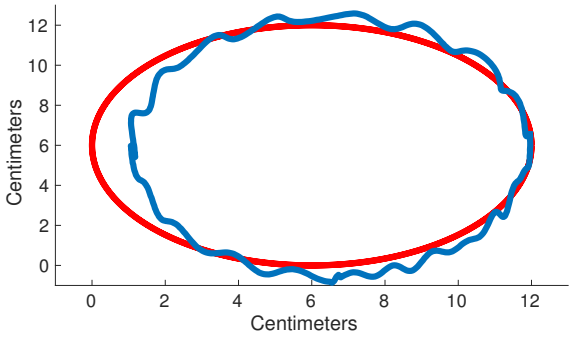


Fig. 9. Simulation of the closed-loop controlled trajectory tracking, showing the end-effector position. Zero on both axes is the position when the arm is in its straight resting pose. The red line is the reference signal and the blue line is the output of the simulation.

## IV. CLOSED-LOOP EXPERIMENTS ON PROTOTYPE

In this section, we validate the control algorithm presented in the previous section through physical experiments on an actual prototype. We start by first describing the fabrication of our soft robotic arm and explaining the experimental setup of the pneumatic pressure source and the motion capture system. This is followed by an instantiation of our data-driven approach to model and simulate the robotic arm and make us of this for validating our closed-loop control of the physical prototype.

### A. Experimental Setup

The experimental setup consists of a soft multi-segment arm as well as the actuation and motion capture system.

*1) 3D Ribbed Soft Arm:* The soft robot presented here is composed of three segments with four inflatable cavities per segment. Each segment of the soft arm is 11 cm long and has a diameter of 4.5 cm. The manufacturing steps are outlined in Figure 10. The four wax cores are created through injecting liquefied bleached bees-wax into a rubber mold. The wax cores are removed from the mold, post-processed to remove any unnecessary residue, and then assembled into a 3D printed mold for casting a single arm segment. Silicone Rubber is mixed, degassed and filled into the mold. The mold is disassemble and the resulting segment is placed in an oven to melt out the wax and afterwards cooked under boiling water remove any wax residue. Silicone tubing is then glued into one side and silicone rod stock is used to close up the other end of the arm segment. Two more arm segments are manufactured in the same manner. Finally, all silicone tubing is routed so that all three segments can be properly concatenated and glued together. Finally, all tubing is labeled and motion capture markers are added.

*2) Actuation and Motion Capture:* The independent pneumatic actuation of the arm segments is achieved through an array of 12 pressure-controlled proportional valves. A motion tracking system provides real-time measurements of marked points along the in-extensible back of the soft arm. A rigid

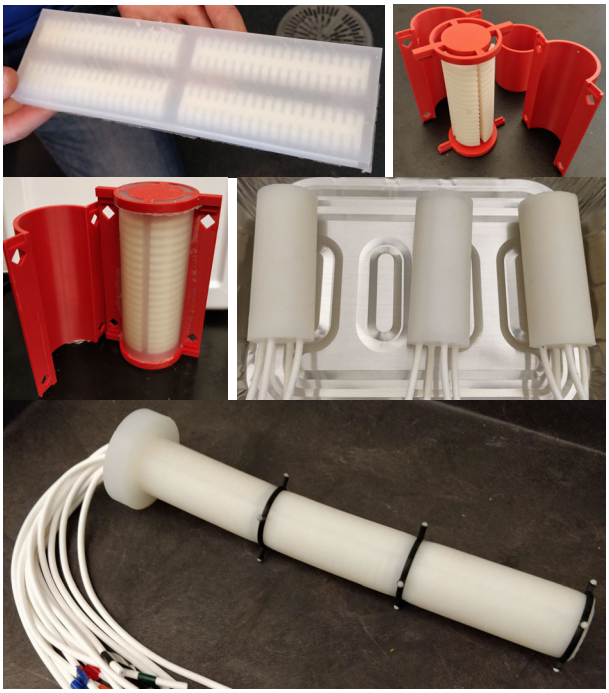

Fig. 10. Manufacturing overview of the 3D soft arm. From Top Left to Bottom Right: Creation of four wax cores through casting; assembly of wax cores into 3D printed molds; casting of Silicone Rubber into the mold; Removal of wax through melting and addition of silicone tubing; Routing of tubing, gluing, labeling and adding markers.

frame holds all the sub-systems together providing reliable hardware experiments without the need for re-calibration of the infrared cameras of the motion capture system.

*3) FEM Setup:* The simulation of the arm uses a finite element mesh made of $45116$ tetrahedra and $11810$ nodes, leading to a state vector of dimensions $11810 \times 6 = 70860$. The simulated model is non-linear, but it is linearized around its resting position in order to design the dynamic controller.

### B. Experimental Validation

For the experimental validation, we perform system identification, pose-to-pose control and trajectory tracking on the physical prototype.

*1) Mechanical Parameter Identification:* To build a precise simulation, elastic and inertial parameters have to be tuned in simulation. The Young's modulus of the structure is directly obtained from silicone's properties and the mass of the arm is measured experimentally. The Rayleigh damping parameters are then tuned experimentally. A comparison between the simulated model and the real arm is given in Section II-D.

*2) Pose-to-Pose Control:* The pose-to-pose control was first tested in simulation as described in Section III-B.1. Here we show the results when we executed the controller on the real robot. A closed loop controlled pose-to-pose motion starting from an actuated state and going to the straight resting pose is shown in Figure 11. Compare this to the open-loop controlled scenario shown in Figure 4. The ITAE and 3% settling time are gathered in Table II to compare the

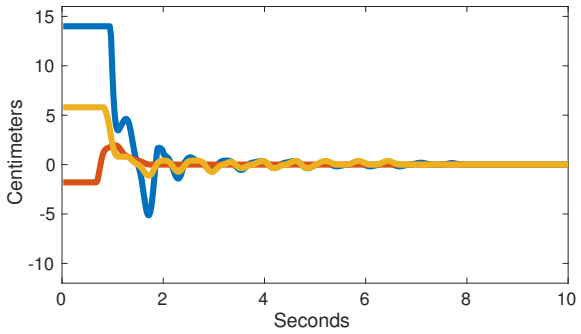


Fig. 11. Closed-loop experiment on real prototype, measuring the end-effector position. Red, blue and yellow lines show the position along the x, y and z axis.

open-loop against the closed-loop experiment. The results show an improvement of $57\%$ in the ITAE metric and an improvement of $49.62\%$ in the $3\%$ settling time metric. The difference between the simulated and experimental results are visible; the gains in the experiments are lower than the gains found in simulation, but it still shows that the controller clearly improves the performance of the system.

TABLE II

OPEN AND CLOSED-LOOP EXPERIMENTS, COMPARING INTEGRAL TIME ABSOLUTE ERROR (ITAE) AND 3% SETTLING TIME FOR EACH.

| | to rest position | to curled position |
|---|---|---|
| ITAE in: | | |
| open-loop | 691.52 | 242.19 |
| closed-loop | 297.33 | 218.95 |
| difference in % | 57 % | 9.6 % |
| 3% settling time in: | | |
| open-loop | 6.53 s | 3.52 s |
| closed-loop | 3.29 s | 2.21 s |
| difference in % | 49.62 % | 37.22 % |

*3) Trajectory Tracking:* Finally, a circular trajectory towards one side of the resting arm pose is defined as the reference input signal for the closed-loop controller. The results are shown in Figure 12. Again, we observe that the actual results are different from the outputs of the simulation. We measure for the closed-loop controlled arm a maximal absolute error of $2.71$ centimeters between the reference trajectory and actual position of the end-effector. In comparison to the simulated scenario described in Section III-B.2, the maximal absolute error was at $1.175$ centimeters.

## V. CONCLUSION

This paper presents both the design of a 3D soft arm using ribbed cavities and the validation of a FEM-based control algorithm. The soft arm is made of silicone elastomer through lost-wax casting. The arms interior cavities are actuated through an array of pneumatic proportional valves. A

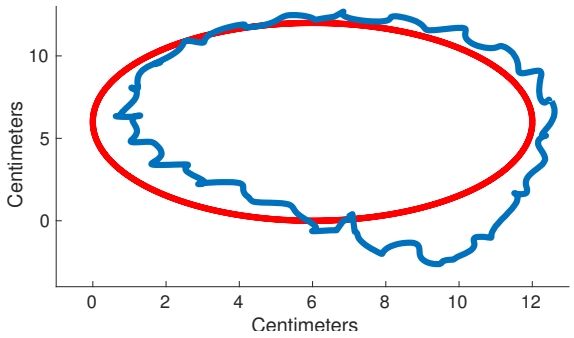


Fig. 12. Physical Experiment of the closed-loop controlled system showing the measurement of the end-effector position. The red line is the reference and the blue line is the real measurement.

motion capture system provides measurement of intermediate points along the soft arm. The soft system allows us to adapt and validate the control methodology presented in [15]. We use a finite element method to build a dynamical model of the robot. We use model order reduction and solve a Linear Matrix Inequalities problem to design a dynamic controller with a state observer.

In this work, we showed that our closed-loop control approach has significant improvements over open-loop actuation, both when performing pose-to-pose control as well as trajectory tracking of a circle. Nevertheless, the experimental results presented here leave room for improvements. We are aware of three possible reasons for the remaining tracking errors presented in the experiments. First, we have not provided a full proof that our control approach is valid for the trajectory tracking experiments. It would require a complete analysis of the dynamics of the large dimensional closed-loop system as it is evolving along the trajectory. This question is the topic of our current research. Second, the control methodology used in this work is based on a linear model. For all experiments conducted in this paper, the model has been linearized at the straight resting shape of the soft robot. This is a known limitation of this approach and we are currently investigating the use of a Linear Parameter Varying (LPV) model to achieve further performance improvements. Third, our proposed method assumes that the soft robot's properties and performance will remain the same with time since an offline simulation is needed beforehand. In reality, however, the material properties of the soft robot may exhibit time-varying properties such as fatigue.

## ACKNOWLEDGMENT

NSF 1830901 and 1226883 This research was conducted at MIT with support from the National Science Foundation (grant NSF 1830901, NSF 1226883). This research was in collaboration with researchers from the DEFROST team at INRIA, with support of ANR (Project ANR-17-ERC2-0029), the European Union through the European Regional Development Fund (ERDF), the French Ministry of Higher Education and Research, the National Center for Scientific Research (CNRS), and the Hauts-de-France Region. We are grateful for these supports.

## REFERENCES

[1] D. Rus and M. T. Tolley, "Design, fabrication and control of soft robots," *Nature*, vol. 521, no. 7553, pp. 467–475, 2015.

[2] R. K. Katzschmann, J. Delpreto, R. MacCurdy, and D. Rus, "Exploration of underwater life with an acoustically-controlled soft robotic fish," *Science Robotics*, vol. 3, no. 16, 2018.

[3] R. Deimel and O. Brock, "A novel type of compliant and underactuated robotic hand for dexterous grasping," *The International Journal of Robotics Research*, vol. 35, no. 1-3, pp. 161–185, 2016.

[4] S. Seok, C. D. Onal, K.-J. Cho, R. J. Wood, D. Rus, and S. Kim, "Meshworm: a peristaltic soft robot with antagonistic nickel titanium coil actuators," *IEEE/ASME Transactions on mechatronics*, vol. 18, no. 5, pp. 1485–1497, 2013.

[5] C. Laschi, M. Cianchetti, B. Mazzolai, L. Margheri, M. Follador, and P. Dario, "Soft robot arm inspired by the octopus," *Advanced Robotics*, vol. 26, no. 7, pp. 709–727, 2012.

[6] D. Trivedi, A. Lotfi, and C. D. Rahn, "Geometrically exact models for soft robotic manipulators," *IEEE Transactions on Robotics*, vol. 24, no. 4, pp. 773–780, 2008.

[7] T. G. Thuruthel, E. Falotico, M. Manti, and C. Laschi, "Stable open loop control of soft robotic manipulators," *IEEE Robotics and Automation Letters*, vol. 3, no. 2, pp. 1292–1298, 2018.

[8] M. T. Gillespie, C. M. Best, E. C. Townsend, D. Wingate, and M. D. Killpack, "Learning nonlinear dynamic models of soft robots for model predictive control with neural networks," in *2018 IEEE International Conference on Soft Robotics (RoboSoft)*, April 2018, pp. 39–45.

[9] C. Della Santina, R. K. Katzschmann, A. Bicchi, and D. Rus, "Dynamic control of soft robots interacting with the environment," in *2018 IEEE International Conference on Soft Robotics (RoboSoft)*, Livorno, Italy, Mar 2018.

[10] R. K. Katzschmann, C. Della Santina, Y. Toshimitsu, A. Bicchi, and D. Rus, "Dynamic motion control of multi-segment soft robots using piecewise constant curvature matched with an augmented rigid body model," in *2019 IEEE International Conference on Soft Robotics (RoboSoft)*, Seoul, South Korea, Apr 2019.

[11] J. Allard, S. Cotin, F. Faure, P.-J. Bensoussan, F. Poyer, C. Duriez, H. Delingette, and L. Grisoni, "Sofa-an open source framework for medical simulation," in *MMVR 15-Medicine Meets Virtual Reality*, vol. 125. IOP Press, 2007, pp. 13–18.

[12] E. Coevoet *et al.*, "Software toolkit for modeling, simulation and control of soft robots," *Advanced Robotics, TaylorFrancis, pp.1-26*, 2017.

[13] J. Chenevier, D. González, J. V. Aguado, F. Chinesta, and E. Cueto, "Reduced-order modeling of soft robots," *PloS one*, vol. 13, no. 2, p. e0192052, 2018.

[14] O. Goury and C. Duriez, "Fast, generic, and reliable control and simulation of soft robots using model order reduction," *IEEE Transactions on Robotics*, no. 99, pp. 1–12, 2018.

[15] M. Thieffry, A. Kruszewski, C. Duriez, and T.-M. Guerra, "Control design for soft robots based on reduced order model," *Robotics and Automation Letters*, 2018.

[16] R. K. Katzschmann, A. D. Marchese, and D. Rus, "Hydraulic Autonomous Soft Robotic Fish for 3D Swimming," in *2014 International Symposium on Experimental Robotics (ISER 2014)*, vol. 109, no. 1122374, Marrakech, Morocco, 2014, pp. 405–420.

[17] B. S. Homberg, R. K. Katzschmann, M. R. Dogar, and D. Rus, "Haptic Identification of Objects using a Modular Soft Robotic Gripper," in *Intelligent Robots and Systems (IROS), 2015 IEEE/RSJ International Conference on*, sep 2015, pp. 1698–1705.

[18] ——, "Robust proprioceptive grasping with a soft robot hand," *Autonomous Robots*, Apr 2018.

[19] A. D. Marchese, R. K. Katzschmann, and D. Rus, "A Recipe for Soft Fluidic Elastomer Robots," *Soft Robotics*, vol. 2, no. 1, pp. 7–25, 2015. [Online]. Available: http://online.liebertpub.com/doi/10.1089/soro.2014.0022

[20] R. K. Katzschmann, A. D. Marchese, and D. Rus, "Autonomous Object Manipulation Using a Soft Planar Grasping Manipulator," *Soft Robotics*, vol. 2, no. 4, pp. 155–164, dec 2015. [Online]. Available: http://online.liebertpub.com/doi/10.1089/soro.2015.0013

[21] A. D. Marchese and D. Rus, "Design, kinematics, and control of a soft spatial fluidic elastomer manipulator," *The International Journal of Robotics Research*, vol. 35, no. 7, pp. 840–869, 2016.

[22] P. Benner, A. Cohen, M. Ohlberger, and K. Willcox, *Model reduction and approximation: theory and algorithms*. SIAM, 2017, vol. 15.